Helical Luttinger Liquid in Topological Insulator Nanowires

R. Egger,[1,2] A. Zazunov,[1] and A. Levy Yeyati[2]

[1]*Institut für Theoretische Physik, Heinrich-Heine-Universität, D-40225 Düsseldorf, Germany*

[2]*Departamento de Física Teórica de la Materia Condensada C-V, Universidad Autónoma de Madrid, E-28049 Madrid, Spain*

(Received 23 June 2010; published 23 September 2010)

We derive and analyze the effective low-energy theory for interacting electrons in a cylindrical nanowire made of a strong topological insulator. Three different approaches provide a consistent picture for the band structure, where surface states forming inside the bulk gap correspond to one-dimensional bands indexed by total angular momentum. When a half-integer magnetic flux pierces the nanowire, we find a strongly correlated helical Luttinger liquid topologically protected against weak disorder. We describe how transport experiments can detect this state.

DOI: 10.1103/PhysRevLett.105.136403 PACS numbers: 71.10.Pm, 73.23.−b, 73.63.−b

The rich and fascinating physics found in certain spin-orbit coupled materials exhibiting the "strong topological insulator" (TI) phase currently attracts an enormous amount of attention [1]. In a TI the bulk has a finite gap Δ_b but topologically protected surface modes exist inside the gap. Using Bi_2Se_3, which presently is the reference material due to its rather large gap, $\Delta_b \approx 0.3$ eV, surface probe experiments (ARPES, STM) have provided clear evidence for the theoretically predicted massless Dirac fermion surface state with spin and momentum locked together [2]. However, probing the surface state in transport experiments still poses a major challenge because residual bulk charge carriers—either related to disorder or due to unintentional intrinsic doping—tend to mask the surface contribution even in the cleanest samples so far available [3]. The surface contribution is easier to extract experimentally in thin-film geometries [4] or in TI nanowires [5,6], where the surface-to-volume ratio is more advantageous. In the latter case, introduction of a magnetic flux Φ piercing the nanowire resulted in an Aharonov-Bohm effect caused by the surface state.

These recent developments clearly demonstrate the need for a comprehensive effective low-energy theory of the electronic properties of TI nanowires, which we formulate here. Very recent work [7,8] has addressed the effect of strong disorder for the noninteracting problem. We instead consider the weak disorder limit but take into account electron-electron (e-e) interactions in a nonperturbative way. We obtain the band structure of a cylindrical TI nanowire from three different approaches: (i) using the low-energy approach of Zhang *et al.* [9], (ii) from the distorted diamond lattice model with spin-orbit couplings introduced by Fu *et al.* [10], and (iii) using a surface Dirac fermion theory [11,12]. Taken together, these calculations draw a consistent picture for the surface states inside the bulk gap, even for very thin nanowires: a one-dimensional (1D) electron waveguide with modes indexed by the half-integer total angular momentum j is formed, where each mode contains a right and a left mover. The spin direction is always tangential to the surface and perpendicular to the momentum. For integer flux Φ (in units of the flux quantum), we have an even number of *massive* 1D Dirac fermion modes, unlike the case of carbon nanotubes [13,14]. This allows for impurity backscattering, and with e-e interactions one has standard disordered Luttinger liquid (LL) behavior [15,16], where the $SU(2)$ spin symmetry is broken. The case of half-integer Φ is more intriguing. Here an emergent time reversal symmetry for the surface states results in an odd number of modes topologically protected against weak disorder. With interactions this yields a *helical Luttinger liquid*. In the simplest single-mode case, the spin polarization of a right (left) mover has a counterclockwise (clockwise) orientation around the waist of the cylinder. The helical LL has been described previously [17,18] as edge mode of the 2D "quantum spin Hall" (QSH) topological insulator realized in HgTe/CdTe quantum well structures [19]. However, it has been difficult to reveal the QSH helical LL experimentally, since usually the edges living on opposite boundaries both contribute. While more complicated setups involving junctions of different QSH systems have been suggested [20], the situation is unique for a TI nanowire at half-integer Φ: the fermion doubling theorem [17] is circumvented and, effectively, just one QSH edge can be realized. This simpler realization of a helical LL should allow for clear signatures in transport experiments.

Let us start with the band structure of a clean noninteracting cylindrical nanowire for $\Phi = 0$. First, we employ the low-energy approach of Zhang *et al.* [9] where, expanding up to order $\boldsymbol{k}^2$ in momentum around a suitable symmetry point, e.g., the Γ point in Bi_2Se_3, the bulk TI Hamiltonian consistent with time reversal symmetry plus inversion and rotation symmetry has the form

$$H_Z = \epsilon_0(\boldsymbol{k})\sigma_0\tau_0 + M(\boldsymbol{k})\sigma_0\tau_z + A_1 k_z \sigma_z\tau_x + A_2\tau_x(k_x\sigma_x + k_y\sigma_y). \quad (1)$$

The z direction defines the anisotropy axis, $\epsilon_0(\boldsymbol{k}) = C + D_1 k_z^2 + D_2 k_\perp^2$, $M(\boldsymbol{k}) = M_0 + B_1 k_z^2 + B_2 k_\perp^2$, and $k_\perp^2 = k_x^2 + k_y^2$. We use Pauli matrices $\boldsymbol{\sigma}$ for spin and $\boldsymbol{\tau}$ for parity (orbital) space; σ_0 and τ_0 denote the identity. The TI phase is realized for $M_0 B_{1,2} < 0$, and we take parameters for Bi_2Se_3 as quoted in Ref. [9]. For a nanowire along the $\hat{e}_z$ direction [we use cylindrical coordinates with unit vectors $\hat{e}_r = (\cos\phi, \sin\phi, 0)$ and $\hat{e}_\phi = (-\sin\phi, \cos\phi, 0)$, and put $\hbar = 1$], rotation symmetry in the xy plane implies conservation of total angular momentum $J_z = -i\partial_\phi + \sigma_z/2$, with half-integer eigenvalues j. For nanowire radius R, we require the wave function to vanish at the boundary $r = R$, which is automatically ensured by expanding in the orthonormal set of radial functions [21]

$$u_{mn}(r < R) = \frac{\sqrt{2}}{R J_{m+1}(\gamma_{mn})} J_m\left(\gamma_{mn}\frac{r}{R}\right),$$

where γ_{mn} is the nth zero of the Bessel function J_m with integer m. For given $(k \equiv k_z, j)$, we express H_Z in the basis $|n, \sigma, \tau\rangle$, where $\sigma = \pm(\tau = \pm)$ denotes the eigenvalue of σ_z (τ_z) and the associated radial function is $u_{j-\sigma/2,n}(r)$. Some algebra gives

$$H_Z|n\sigma\tau\rangle = (\epsilon_0(k) + M(k)\tau)|n\sigma\tau\rangle + A_1 k\sigma|n, \sigma, -\tau\rangle + \frac{2iA_2}{R}\sum_{n'}\frac{\gamma_{j+\sigma/2,n'}\gamma_{j-\sigma/2,n}}{\gamma_{j+\sigma/2,n'}^2 - \gamma_{j-\sigma/2,n}^2}|n', -\sigma, -\tau\rangle \quad (2)$$

with the substitution $k_\perp \to \gamma_{j-\sigma/2,n}/R$ in $\epsilon_0(\boldsymbol{k})$ and $M(\boldsymbol{k})$. Numerical diagonalization then yields topologically protected surface modes. A typical band structure and spin (particle) density profiles are shown in Fig. 1. Evidently all surface modes have a finite gap. States with (k, j) and $(-k, -j)$ form a Kramers degenerate pair, and for given k, the $\pm j$ states are degenerate but have opposite s_z spin polarization. We observe that the expectation values of the spin density operators $s_{\phi,r,z} \equiv \frac{1}{2}\hat{e}_{\phi,r,z}\cdot\boldsymbol{\sigma}$ only depend on the radial coordinate r. Since then $\langle s_r\rangle = -\partial_\phi\langle s_\phi\rangle = 0$, spin is always oriented tangential to the surface. Moreover, the spin direction always encloses the angle $\eta = \pi/2$ with the momentum $\boldsymbol{k} = k\hat{e}_z + (j/R)\hat{e}_\phi$. For large $|k|$, a right (left) moving surface state then has counterclockwise (clockwise) spin polarization $\langle s_\phi\rangle > 0$ ($\langle s_\phi\rangle < 0$).

More microscopically, a TI nanowire can be described by a tight-binding model for the electronic states in a diamond lattice with spin-orbit coupling λ_{so} [10],

$$H_{tb} = \sum_{\langle i,j\rangle} t_{ij} c_i^\dagger c_j + \frac{4i\lambda_{so}}{a^2}\sum_{\langle\langle i,j\rangle\rangle} c_i^\dagger(\boldsymbol{\sigma}\cdot[\boldsymbol{d}_{ij}^1 \times \boldsymbol{d}_{ij}^2])c_j, \quad (3)$$

where a is the lattice spacing. To reach the TI phase, a distortion $t_{ij} \to t_{ij} + \delta t$ in the nearest-neighbor hopping is introduced along the (111) direction. The λ_{so} term involves second neighbors and depends on the two nearest-neighbor vectors $\boldsymbol{d}^{1,2}$ connecting them. After choosing an axis direction ($\hat{e}_z$), the wire is formed by all lattice sites located within radius R. A typical band structure for a nanowire with $R = 5a$ and $\hat{e}_z$ in the (111) direction is shown in Fig. 2. The surface states are again characterized by a finite gap, and spin or particle densities are qualitatively consistent with those shown in the inset of Fig. 1. The radius dependence of the lowest surface state gap, $\Delta_s(R)$, obtained under both approaches is compared in Fig. 3, where we set the parameter $-2t + \delta t$ in H_{tb}, which is half the gap in the (111) direction, equal to M_0 in Eq. (1). Agreement between both models at large R is reached by adjusting a to 2.8 nm. We see that even for very thin nanowires, the analytical prediction $\Delta_s = v_2/R$, see Eq. (5) below, agrees very well with the tight-binding result, while the low-energy model (2) gives deviations when $R < 5$ nm. Even though a $\boldsymbol{k}\cdot\boldsymbol{p}$ expansion of H_{tb} around the $L = \frac{\pi}{a}(1, 1, 1)$ point does not match completely with Eq. (1), the main features of the surface states are equivalent in both

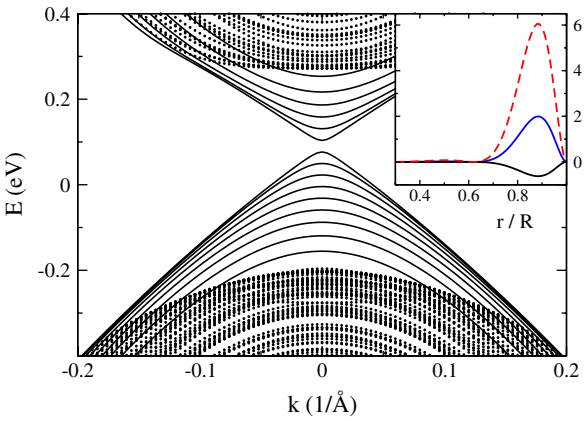

FIG. 1 (color online). Band structure of a TI nanowire with $R = 15$ nm obtained by numerical diagonalization of Eq. (2). Points refer to bulk states, lines to surface states. Inset: Density $\langle\rho\rangle$ (dashed red line) and spin density [$\langle s_\phi\rangle$; blue solid line, $\langle s_z\rangle$; black curve] vs radial coordinate for the right-moving state $(k, j) = (0.02\ \text{Å}^{-1}, 1/2)$.

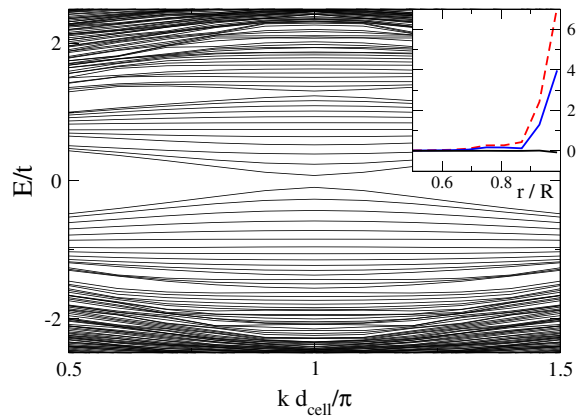

FIG. 2 (color online). Same as Fig. 1 but using the tight-binding model on a diamond lattice, see Eq. (3). We take $\hat{e}_z$ along the (111) axis, $R = 5a$, $\lambda_{so} = t$, and $\delta t = 0.28t$. The size of the unit cell along this direction is $d_{cell} = \sqrt{3}a$. Inset: as in Fig. 1 but for $kd_{cell} = 2.9$.

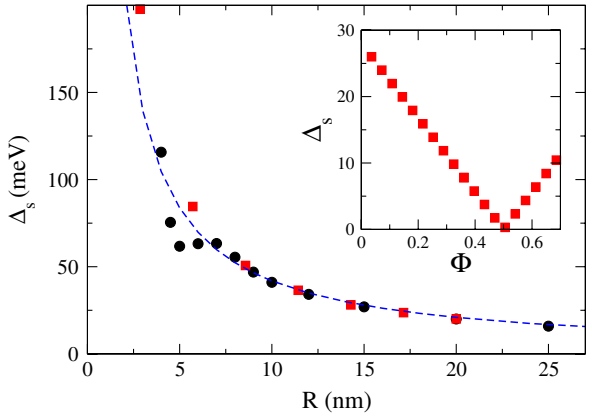

FIG. 3 (color online). Numerical results for the lowest surface state gap Δ_s vs nanowire radius R, obtained from the low-energy approach (2) [black circles] and from the tight-binding model (3) [red squares]. The analytical prediction v_2/R, see Eq. (5), is given as a blue dashed curve. Inset: Φ dependence of Δ_s for $R = 5a$ from the tight-binding approach, where the flux is introduced via Peierls phases.

descriptions. Similar results are obtained when $\hat{e}_z$ points along other crystallographic directions.

Both the dispersion relation and the spin texture of the surface states found under these two approaches are well reproduced by a model of 2D massless Dirac fermions wrapped onto the cylinder surface, under the condition that the spin is tangential to the surface and perpendicular to the momentum ($\eta = \pi/2$), cf. Ref. [11]. To match the above numerical results, we also need to take into account anisotropy, since there are different Fermi velocities $v_{1,2}$ along the $\hat{e}_{z,\phi}$ directions. By supplementing Eq. (1) with boundary conditions describing a flat 2D surface in the xz plane, we find $v_{1,2} = A_{1,2}\sqrt{1 - (D_2/B_2)^2}$. Taking the parameters of Ref. [9] for Bi_2Se_3, $v_2/v_1 \approx 2$. With $\eta = \pi/2$, the surface Hamiltonian takes the form [11]

$$H_{\text{surf}} = e^{-i\sigma_z\phi/2}\left(v_1 k\sigma_y - \frac{v_2}{R}\sigma_z(-i\partial_\phi + \Phi)\right)e^{i\sigma_z\phi/2}, \tag{4}$$

where we added the dimensionless flux parameter Φ. We note that Φ may include not only the orbital magnetic field, but also a Zeeman field or an exchange-coupled magnetization due to a nearby magnet (for fields along $\hat{e}_z$). The dispersion relation implied by Eq. (4) is

$$E_{k,j,\pm} = \pm\sqrt{v_1^2k^2 + \frac{v_2^2(j+\Phi)^2}{R^2}}, \tag{5}$$

where the $\pm$ sign refers to conduction and valence band, respectively. The corresponding eigenstate is

$$\psi_{k,j,\pm}(z,\phi) \sim e^{ikz+ij\phi}e^{-i\sigma_z\phi/2}\begin{pmatrix} u_{k,j,\pm} \\ \pm i\sqrt{1-u_{k,j,\pm}^2}\end{pmatrix},$$
$$u_{k,j,\pm} = \frac{v_1 k}{\sqrt{2E_{k,j,\pm}[E_{k,j,\pm} + (j+\Phi)v_2/R]}}. \tag{6}$$

For integer Φ, all bands are doubly degenerate and have a gap $\geq \Delta_s = v_2/R$. The mass term in the relativistic dispersion (5) comes from a Berry phase π due to spin-surface locking [11,12]. While scattering between Kramers pairs, $(k, j+\Phi) \leftrightarrow [-k, -(j+\Phi)]$, is forbidden since the states (6) have zero overlap, backscattering ($k \to -k$) for fixed j is allowed; i.e., potential scattering (disorder) is relevant. A noninteger flux Φ lifts the degeneracy, and for half-integer Φ, the mass appearing in Eq. (5) vanishes for the special band $j = -\Phi$. This feature also appears in the tight-binding calculation, see inset in Fig. 3. Spin-conserving single-particle backscattering processes are then forbidden, and weak disorder has no effect [22]. When the chemical potential μ is inside the bulk gap, we are thus guaranteed to have an *odd* number of modes.

In the remainder, we focus on half-integer Φ. For simplicity, we consider $\mu < \Delta_s$ and sufficiently weak interactions, where only the single mode $j = -\Phi$ needs to be retained in a low-energy effective theory. Moreover, we assume $\mu > 0$ so that umklapp e-e scattering can also be neglected, cf. Ref. [17]. Using the spinors (6), the surface electron operator $\Psi(z,\phi)$ is expanded in terms of slowly varying chiral 1D fermions $\psi_{r=\pm}(z)$,

$$\Psi(z,\phi) = \frac{1}{\sqrt{4\pi}}\sum_{r=\pm} e^{irk_F z}\psi_r(z)\begin{pmatrix} r \\ ie^{i\phi}\end{pmatrix}, \tag{7}$$

with the Fermi momentum $k_F \equiv \mu/v_1$. The standard bosonization approach [15] expresses $\psi_r(z) \simeq (2\pi\xi)^{-1/2} \times \exp[i\sqrt{\pi}(\varphi + r\theta)]$ in terms of conjugate phase fields $\varphi(z)$ and $\theta(z)$, where the surface layer width ξ is the short distance cutoff for the 1D continuum description. The noninteracting Hamiltonian is $H_0 = \frac{v_1}{2}\int dz[(\partial_z\varphi)^2 + (\partial_z\theta)^2]$. The density operator, $\rho(z,\phi) = \Psi^\dagger\Psi$, is then equal to the 1D density, $\partial_z\theta/\sqrt{\pi}$. Similarly, the spin density operators s_ϕ and s_z are reduced to a 1D form,

$$\begin{pmatrix} s_\phi \\ s_z\end{pmatrix} \equiv \frac{1}{2}\Psi^\dagger(z,\phi)\begin{pmatrix}\sigma_y e^{i\phi\sigma_z} \\ \sigma_z\end{pmatrix}\Psi(z,\phi)$$
$$= \begin{pmatrix} J(z) \\ -\frac{1}{\pi\xi}\cos[2k_F z + 2\sqrt{\pi}\theta(z)]\end{pmatrix}. \tag{8}$$

We observe that s_ϕ equals the 1D current density, $J(z) \equiv \partial_z\varphi/\sqrt{\pi}$, reflecting spin-momentum locking. There are no $2k_F$ oscillatory terms in ρ nor in s_ϕ. On the other hand, no "slow" terms exist for s_z, and we always have $\langle s_z\rangle = 0$.

We now include e-e interactions, assuming that no metallic gates are nearby. Similar to the nanotube case, apart from a hard-core part, the main contribution to the (surface-projected) potential can be modeled by [14]

$$U(\boldsymbol{r} - \boldsymbol{r}') = \frac{e^2/\kappa}{\sqrt{(z-z')^2 + \xi^2 + 4R^2\sin^2[(\phi-\phi')/2]}},$$

where κ takes into account the dielectric constant of the substrate and of the insulating interior part of the nanowire.

Inserting the field operator (7) into the general second-quantized interaction Hamiltonian yields the 1D expression

$$H_{e-e} = \frac{1}{2\pi}\int dz dz' V(z-z')\partial_z\theta(z)\partial_{z'}\theta(z') \qquad (9)$$

with the effective 1D potential $V(z) = (2\pi)^{-1}\times \int_0^{2\pi} d\phi U(z,\phi)$. The explicit form of V is given in Ref. [14] and has the Fourier transform $\tilde{V}(q) \simeq (2e^2/\kappa)\times [0.51 - \ln|qR|]$ for $|q|R \ll 1$. Hard-core interaction terms give an additional contribution $b\int dz[(\partial_z\theta)^2 - (\partial_z\phi)^2]$ to the Hamiltonian, where b depends on microscopic details. Since b stays marginal under renormalization group transformations, the logarithmic singularity in $\tilde{V}(q)$, caused by the long-ranged Coulomb tail, is expected to dominate in practice. Approximating $q \approx 2\pi/L$ for nanowire length L, we obtain the single-mode helical LL [17], $H_{\mathrm{hLL}} = \frac{v}{2}\int dz[K(\partial_z\phi)^2 + K^{-1}(\partial_z\theta)^2]$, where $v = v_1/K$ and

$$K = \frac{1}{\sqrt{1+\frac{2e^2}{\pi\kappa v_1}(\ln[L/(2\pi R)]+0.51)}}, \qquad (10)$$

with $K = 1$ without interactions. It is straightforward to generalize these expressions to $b \neq 0$ [15,20]. For $L/R \approx 1000$, we find the strongly correlated value $K \approx 0.4$ to 0.5 from Eq. (10). We note that $K \approx 0.53$ to 0.9 [20] for the QSH edge in HgTe/CdTe wells.

The helical LL state in a TI nanowire can be identified through several experimentally observable signatures. First, we note that the equal-time spatial correlations of ρ and $s_\phi = J$ decay as $|z|^{-2}$. While $\langle s_z\rangle = 0$ remains valid for arbitrary K, s_z correlations show a slow algebraic power-law decay, $\langle s_z(z)s_z(0)\rangle \propto \cos(2k_F z)|z|^{-2K}$. For $K < 1$, we therefore find an ordering tendency towards spin density wave formation, where spins are oriented along the nanowire axis $\hat{e}_z$. Within the standard classification of 1D systems [15], the helical LL in a TI nanowire is thus in a spin density wave phase. As a consequence, the Ruderman-Kittel interaction among magnetic impurities is extremely anisotropic [23] and decays only with a slow power law. At the same time, the absence of $2k_F$ terms in the density operator implies that no charge density wave correlations develop at all. Furthermore, the superconducting order parameter describing singlet Cooper pairing is $\mathcal{O}(z,\phi) \sim e^{i\phi}\psi_+(z)\psi_-(z)$, which implies a fast power-law decay $\propto |z|^{-2/K}$. The angular $e^{i\phi}$ dependence comes from the spin structure in Eq. (7) and causes an additional strong suppression of the proximity effect. For normal-state metallic electrodes, in a two-terminal geometry, the conductance is $G = e^2/h$ (independent of K) when the contacts are ideal. However, nonideal contacts cause a typical temperature-dependent decrease of $G(T)$ at low temperatures due to the well-known power-law suppression of the tunneling density of states [20]. Moreover, in contrast to a spin-polarized LL (which also has $G = e^2/h$ for ideal contacts), spin plays an essential role here. This could be easily seen in the presence of magnetic impurities. In particular, the Kondo effect can take place, where theoretical predictions for $G(T)$ exist [24] and directly apply. To conclude, we are confident that the helical LL will soon allow for its clear experimental identification in topological insulator nanowires.

This work was supported by the SFB TR 12 of the DFG, the ESF network INSTANS, and by the Spanish MICINN under Contract No. FIS2008-04209.

[1] For reviews see: X.-L. Qi and S.-C. Zhang, Phys. Today **63**, 33 (2010); M. Z. Hasan and C. L. Kane, arXiv:1002.3895 [Rev. Mod. Phys. (to be published)].
[2] Y. Xia *et al.*, Nature Phys. **5**, 398 (2009).
[3] N. P. Butch *et al.*, Phys. Rev. B **81**, 241301(R) (2010).
[4] J. G. Checkelsky, Y. S. Hor, R. J. Cava, and N. P. Ong, arXiv:1003.3883.
[5] H. Peng *et al.*, Nature Mater. **9**, 225 (2010).
[6] D. Kong *et al.*, Nano Lett. **10**, 329 (2010).
[7] Y. Zhang and A. Vishwanath, arXiv:1005.3542.
[8] J. H. Bardarson, P. W. Brouwer, and J. E. Moore, arXiv:1005.3762.
[9] H. Zhang, C.-X. Liu, X.-L. Qi, X. Dai, Z. Fang, and S.-C. Zhang, Nature Phys. **5**, 438 (2009).
[10] L. Fu, C. L. Kane, and E. J. Mele, Phys. Rev. Lett. **98**, 106803 (2007).
[11] Y. Zhang, Y. Ran, and A. Vishwanath, Phys. Rev. B **79**, 245331 (2009).
[12] P. M. Ostrovsky, I. V. Gornyi, and A. D. Mirlin, Phys. Rev. Lett. **105**, 036803 (2010).
[13] R. Egger and A. O. Gogolin, Phys. Rev. Lett. **79**, 5082 (1997); C. L. Kane, L. Balents, and M. P. A. Fisher, Phys. Rev. Lett. **79**, 5086 (1997).
[14] R. Egger and A. O. Gogolin, Eur. Phys. J. B **3**, 281 (1998).
[15] A. O. Gogolin, A. A. Nersesyan, and A. M. Tsvelik, *Bosonization and Strongly Correlated Systems* (Cambridge University Press, Cambridge, England, 1998).
[16] T. Giamarchi and H. J. Schulz, Phys. Rev. B **37**, 325 (1988); C. Mora, R. Egger, and A. Altland, Phys. Rev. B **75**, 035310 (2007).
[17] C. Wu, B. A. Bernevig, and S.-C. Zhang, Phys. Rev. Lett. **96**, 106401 (2006).
[18] C. Xu and J. E. Moore, Phys. Rev. B **73**, 045322 (2006).
[19] M. König *et al.*, J. Phys. Soc. Jpn. **77**, 031007 (2008).
[20] C. Y. Hou, E. A. Kim, and C. Chamon, Phys. Rev. Lett. **102**, 076602 (2009); A. Ström and H. Johannesson, Phys. Rev. Lett. **102**, 096806 (2009); J. C. Y. Teo and C. L. Kane, Phys. Rev. B **79**, 235321 (2009).
[21] N. Agrait, A. Levy Yeyati, and J. M. van Ruitenbeek, Phys. Rep. **377**, 81 (2003).
[22] Note that two-particle backscattering effects combined with very strong interactions can destabilize the helical liquid [17,18].
[23] J. Gao, W. Chen, X. C. Xie, and F.-C. Zhang, Phys. Rev. B **80**, 241302(R) (2009).
[24] J. Maciejko, C. Liu, Y. Oreg, X.-L. Qi, C. Wu, and S.-C. Zhang, Phys. Rev. Lett. **102**, 256803 (2009).